Available online at www.sciencedirect.com
SCIENCE DIRECT®

ICARUS

Icarus 177 (2005) 190–195

www.elsevier.com/locate/icarus

Near-IR imaging of Asteroid 4 Vesta

N.E.B. Zellner[a,*], S. Gibbard[a], I. de Pater[b], F. Marchis[b], M.J. Gaffey[c]

[a] *Institute for Geophysics and Planetary Physics, Lawrence Livermore National Laboratory, 7000 East Ave, Livermore, CA 94550, USA*
[b] *Department of Astronomy, 601 Campbell Hall, University of California, Berkeley, CA 94720, USA*
[c] *Department of Space Studies, University of North Dakota, Box 9008, Grand Forks, ND 58202-9008, USA*

Received 11 May 2004; revised 21 March 2005

Available online 25 May 2005

Abstract

The Keck Observatory's adaptive optics (AO) system has been used to observe Asteroid 4 Vesta during its 2003 closest approach to Earth. Broadband K′- and L′-band images, centered at 2.1 and 3.6 μm, respectively, are presented here. The sharpness of the images was improved by applying a deconvolution algorithm, MISTRAL, to the images. The K′- and L′-band images at spatial resolutions of 53 km (0.055″) and 88 km (0.085″), respectively, display albedo features on the surface of the asteroid that can also be seen in the HST images (673 nm) presented by Thomas et al. [1997. Impact excavation on Asteroid 4 Vesta: Hubble Space Telescope results. Science 277, 1492–1495] and Binzel et al. [1997. Geologic mapping of Vesta from 1994 Hubble Space Telescope images. Icarus 128, 95–103] at the same latitudes and longitudes. While we cannot determine the morphology of these features, we can speculate that some of the albedo features may be impact craters filled with dark material. Spectra, centered at 1.65 and 2.1 μm, were also obtained. Spectra were corrected for the solar flux and are similar to those published by Gaffey [1997. Surface lithologic heterogeneity of Asteroid 4 Vesta. Icarus 127, 130–157], along the same wavelength range.

Keywords: Asteroids, Vesta; Surfaces, asteroids; Geological processes; Infrared observations

1. Introduction

Asteroid 4 Vesta, recognized as a differentiated object (McCord et al., 1970) and the potential source of the HED (howardite, eucrite, diogenite) meteorites (e.g., McCord et al., 1970; Larson and Fink, 1975 (near-IR spectrum); Consolmagno and Drake, 1977; Drake, 1979; Thomas et al., 1997; and reviewed thoroughly by Drake, 2001), has been well studied since its discovery in 1807. Multispectral images obtained by the Hubble Space Telescope (HST) in 1994 showed that Vesta is not spherical and possesses regions of differing spectral albedos (Zellner et al., 1997; Binzel et al., 1997). More recent (1996) HST observations showed a south pole depression (crater) 460 ± 3 km wide and 13 ± 3 km deep, and false-color images of this crater show significant color variation that appears correlated with depth; high-calcium pyroxene and olivine are exposed (Thomas et al., 1997), making it reasonable to assume that this crater is the site of origin for the HED meteorites. Previous work determined that the similar textural and mineralogical (Prior, 1916), as well as elemental and isotopic (Clayton and Mayeda, 1996; Papike, 1998), characteristics link these meteorites to a common parental body. In this paper we present near-IR images and spectra of Vesta at a spatial resolution comparable to the visible-light HST images and interpret our data in terms of topography and surface composition.

2. Observations

The Asteroid 4 Vesta was observed on 9 March 2003 (UT) using the W.M. Keck II Telescope with its adaptive optics system (Wizinowich et al., 2000). An example of a raw, unprocessed image can be seen in Fig. 1, top. The Keck AO system consists of a 349-actuator deformable mirror that

* Corresponding author.
E-mail address: zellner1@llnl.gov (N.E.B. Zellner).

0019-1035/$ – see front matter
doi:10.1016/j.icarus.2005.03.024

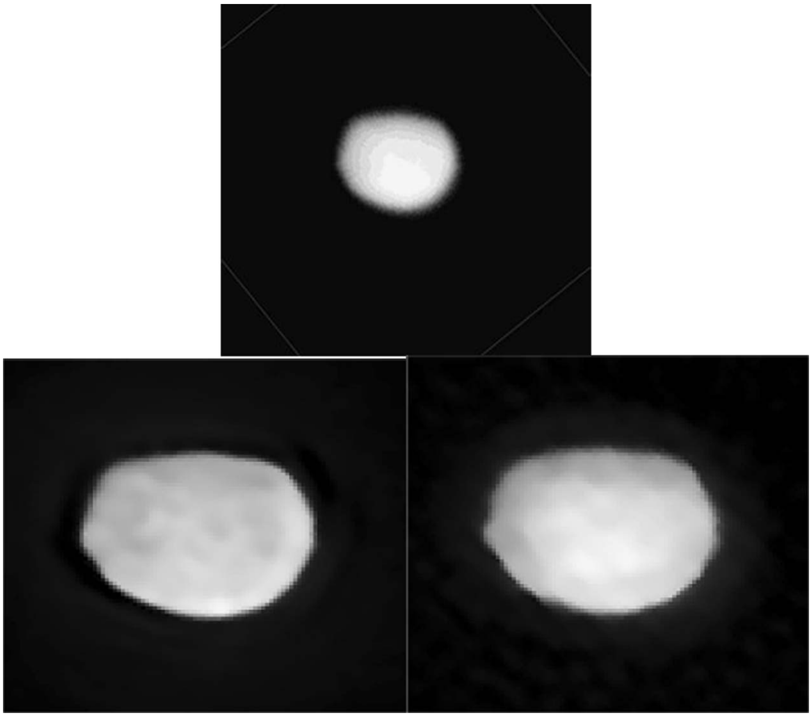

Fig. 1. Top: unprocessed Keck K′-band (2.1 µm) image of Asteroid 4 Vesta. Bottom: processed and deconvolved Keck images of Asteroid 4 Vesta with central longitudes of 37.4° (K′ band, 2.1 µm) (L) and 45.3° (L′ band, 3.6 µm) (R). Spatial resolutions are 53 and 88 km, respectively. North is at the top in all of the images.

Table 1
Observational image data (3/09/03)

Image/spectrum	Filter	Time (UT)	Sub-Earth latitude	Sub-Earth longitude	Sub-solar latitude	Sub-solar longitude	Apparent size (arcsec)	Airmass
Image	K′	8:46	8.15	37.4	16.14	44.24	0.544	1.57
Image	L′	8:53	8.15	45.3	16.14	52.10	0.544	1.53
Spectrum	K′	9:31	8.15	87.99	16.14	94.77	0.544	1.32
Spectrum	H	9:41	8.15	99.22	16.14	106.00	0.544	1.27

operates in a closed-feedback loop using a Shack–Hartmann wavefront sensor. An adaptive optics system corrects for turbulence in the Earth's atmosphere by sampling the wavefront and applying a correction based on the distortion measured for a known source within the same isoplanatic patch as the science target (e.g., a point source such as a star). Small extended objects, such as Vesta, may be used as reference sources for themselves, so no nearby star was required for our observations.

Images at K′ (1.95–2.292 µm) and L′ (3.43–4.13 µm), as well as spectra in the K′ and H (1.48–1.78 µm) bands were taken, as described in Table 1. Spatial resolution (full width at half maximum, FWHM) estimated from observations of stars was 0.055″ for K′ and 0.085″ for L′, compared to Vesta's apparent size of 0.544″. Across Vesta's 530-km disk, we thus had ∼10 resolution elements at K′ and ∼6 resolution elements at L′ (53 and 88 km, respectively). Spectral resolution was $R \sim 2000$. Due to non-photometric seeing conditions, the absolute intensities of the images and spectra are not known.

3. Data analysis/reduction

The image data were reduced according to standard infrared data reduction procedures, including sky subtraction, flat-fielding, and replacement of bad pixels by the median of surrounding pixels. Spectral data were taken as pairs of images shifted along the spectrograph slit; these images were then subtracted to remove the sky background. Reduction of the spectral data was as described in Gibbard et al. (2003), including calibration and division of the spectra by a reference star. In the case of Vesta, in order to obtain reflectance spectra, we performed an additional correction to account for the variation in solar flux with wavelength. Solar flux values were obtained from Colina et al. (1996).

4. Image analysis

A deconvolution algorithm was applied to the images to correct for atmospheric distortion. The Strehl ratio, a common measurement of the quality provided on high angular resolution data, is >20 and up to 75% in the L′ images, indicating good and stable correction. With such a high signal-to-noise ratio, combined with excellent angular resolution, one can expect a significant improvement in the sharpness and sensitivity of the images after applying an a posteriori inversion process such as a deconvolution algorithm. We used MISTRAL (Myopic Iterative STep-preserving Restoration ALgorithm), a deconvolution algorithm developed by ONERA (Office National d'Etudes et de Recherches A'erospatiales) and especially aimed at AO observations of planetary objects (Mugnier et al., 2004). Examples of deconvolved images from this observing run can be seen in Fig. 1, bottom. MISTRAL uses a stochastic approach to find the best image reconstruction, using information about the object and the PSF (point spread function). It requires several star images to evaluate variations in the PSF. The main improvement of this technique over more classical methods is that it avoids both noise amplification and creation of sharp-edged artifacts or "ringing effects," and it better restores the initial photometry (though without a photometric calibration, this is not important for Vesta). This algorithm has been used extensively on simulated and real AO observations (Conan et al., 2000; Marchis et al., 2001), and MISTRAL has provided excellent results for various planetary images recorded at different telescopes (Marchis et al., 2001, 2002; Hestroffer et al., 2002). We have intensively tested the method on real and artificial images, and the resulting image contains considerably fewer artifacts than a classical Lucy–Richardson deconvolved image.

5. Image discussion

L′- and K′-band images with spectra obtained with the Keck AO system are presented here for the first time; we show the images with the locations of the slit spectra indicated on them. Despite the absence of photometric corrections (such as the removal of contributions from reflecting sunlight, considering the shape of the asteroid and the Sun's position), which would have increased the contrast of albedo markings on the surface of Vesta, obvious differences between the two images are clearly seen (Figs. 2 and 3a). Dark features ("A," "B," and "S," from Binzel et al., 1997) can be recognized in the K′-band image but are not as clearly seen in the L′-band image. "Olbers" (Binzel et al., 1997) can be seen in both images. Since all of the patterns are repeatedly observed at both wavelengths, the features are probably real.

We do not have the resolution to determine the morphology of these features, but it is certainly easy to speculate that they may be of impact origin, since impacts have played an important role in Vesta's surface morphology. For example, one possible interpretation for the feature "Olbers" and others larger than 200 km is that they are impact basins that have been filled with basaltic lavas, much in the manner of the lunar maria. This interpretation requires that these features be quite ancient, since the presence of magma on Vesta was likely limited to a very brief period of time within the first few tens of million of years of Solar System history (Mittlefehldt et al., 1998). Continuing the lunar analogy further, high albedo regions may also represent compositional differences, such as higher albedo feldspar-rich eucrite-type assemblages versus lower albedo feldspar-poor assemblages (e.g., diogenites) or lava flows (e.g., Ibiteria-type eucrites).

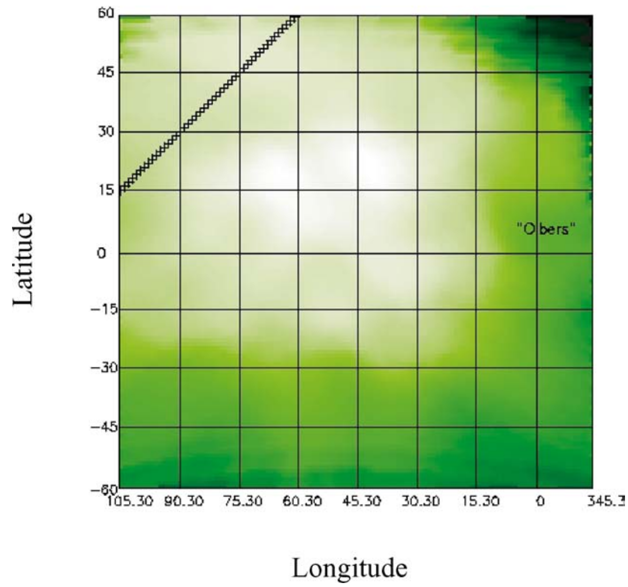

Fig. 2. L′-band (centered at 3.6 μm) image of Asteroid 4 Vesta from 105° to 345° longitude. The bright area centered at 45° longitude may have a depth of 6 km (Thomas et al., 1997). The feature identified as "Olbers" is taken from Binzel et al. (1997). No corrections for limb darkening have been made.

A bright area centered at roughly 45° longitude (and at the sub-solar point) can be seen in the L′-band image (Fig. 2) but is harder to see in the K′-band image (Fig. 3a). Since the same patterns are seen in both the K′- and L′-band images, the brightness difference may be due to different physical properties, such as particle size, of the material; the material may appear bright due to small particles backscattering the reflected sunlight. Alternatively, it may indicate variation in the amount and distribution of pyroxene across the surface. Since there is less contrast in the relative reflectance of feldspar-rich (eucrite) and feldspar-poor (diogenite) basaltic meteorites at wavelengths outside the pyroxene feature (e.g., 3.6 μm) than at wavelengths within the pyroxene feature (e.g., 2.1 μm), a variation in the spatial abundance of pyroxene may produce the lower small scale contrast seen in the 3.6-μm image. A lithologic model can be seen in Fig. 3b. While this feature could indicate an area of thermal emission, calculations for a surface with the albedo and heliocentric distance of Vesta indicate that reflected sunlight exceeds emitted radiation at 3.6 μm by approximately two orders of magnitude and so thermal emission is not significant (see Fig. 4). This large feature is also present in the HST images presented by Thomas et al. (1997) as the dark green area to the right of the 90°-longitude marker (see Fig. 2A

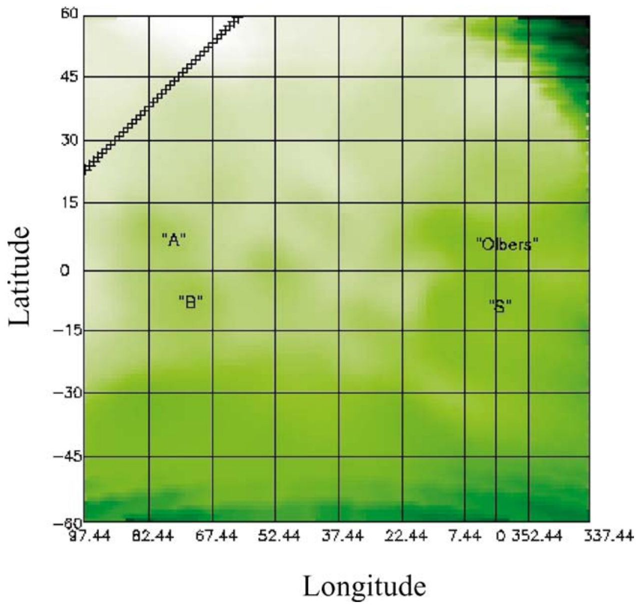

(a)

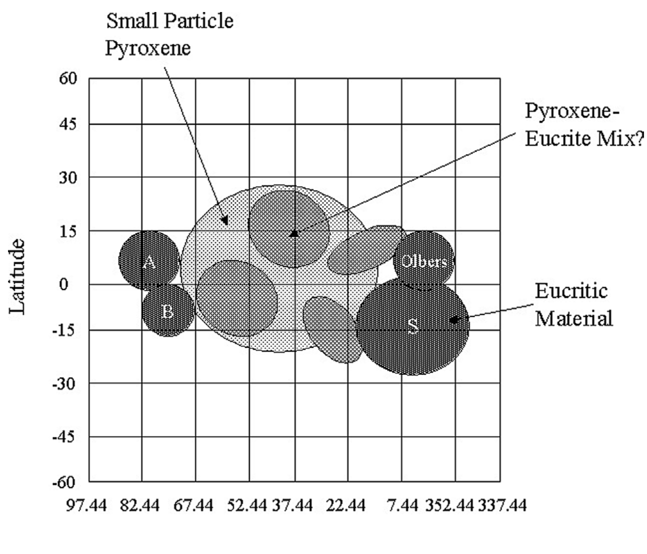

(b)

Fig. 3. (a) K′-band (centered at 2.1 μm) image of Asteroid 4 Vesta from 97° to 337° longitude. The bright area centered at 45° longitude in the L′-band image (Fig. 2) is not so apparent here. The features identified as "A," "B," "S," and "Olbers" are taken from Binzel et al. (1997). No corrections for limb darkening have been made. (b) A possible representation of the major lithologic units present on the surface of Vesta as interpreted from the Keck AO image in the K′ band. Longitudinal positions are well constrained. Units "A," "B," "Olbers," and "S" (from Binzel et al., 1997) are depicted as circles by analogy to impact craters and are probably impact basins with diameters up to 400 km. Units are shown with sharp boundaries but are actually gradational, as seen in Fig. 3a.

in Thomas et al., 1997). Thomas et al. (1997) modeled this feature as having a dynamic depth of 6 km below the mean surface level, indicating a possible impact basin; our data suggest that it is resolved into an area with multiple features. This feature is also seen in data presented by Binzel

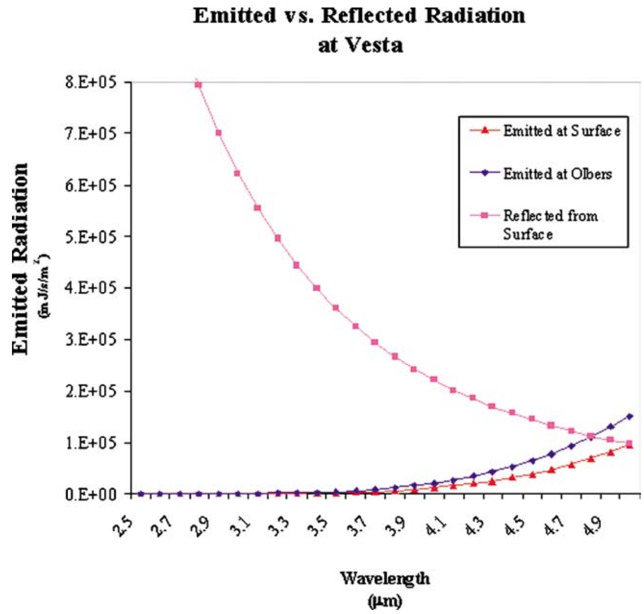

Fig. 4. Plot of emitted vs reflected radiation at the surface of Asteroid 4 Vesta. At 3.6 μm, reflected light dominates and so the bright feature(s) seen in the L′-band image (Fig. 2) is (are) not due to thermal radiation. Emitted radiation begins to exceed reflected light at longer than 4.8 μm at "Olbers" and at longer than 5.1 μm on the surface in general. Calculations were performed with the following assumptions: (1) the reflected and emitted fluxes from the surface element are isotropic; (2) the surface element is flat with no topography and illumination is at normal incidence; and (3) both the Sun and Vesta are blackbody emitters with an emissivity (ε) of 1.0. The temperature used in these calculations was 223 K for the surface and 231 K for "Olbers." A global albedo of 0.42 (visible) was used to determine the solar reflectance values.

et al. (1997) as a red area near the 40°-longitude marker (see Fig. 5). While not labeled specifically in Binzel et al. (1997), the area's red mapping indicates an increasing 1-μm band depth, which may be interpreted as characteristic of mafic features (Binzel et al., 1997), possibly existing below the surface of Vesta.

6. Spectra discussion

Spectra spanning a longitudinal range from 153° to 60° and a latitudinal range from −45° to 60° were also obtained (see Fig. 6). The latitudes and longitudes over which they were recorded have been overlain on the images (dark lines), allowing for spatial resolution at these wavelengths (see Figs. 2 and 3a). All of the spectra, at different disk locations, showed the same spectral curve, implying a compositionally uniform surface at the resolution of our spectra. The same result was also reported as early as 1975 by Larson and Fink (1975). This result is perhaps not surprising since no features at these longitudes and latitudes (and at the stated resolutions) are seen in any of the images presented herein (incl. those from Thomas et al. (1997) and Binzel et al. (1997)). Spectra substantiate previously published data (e.g., Gaffey, 1997) and verify the pyroxene absorption fea-

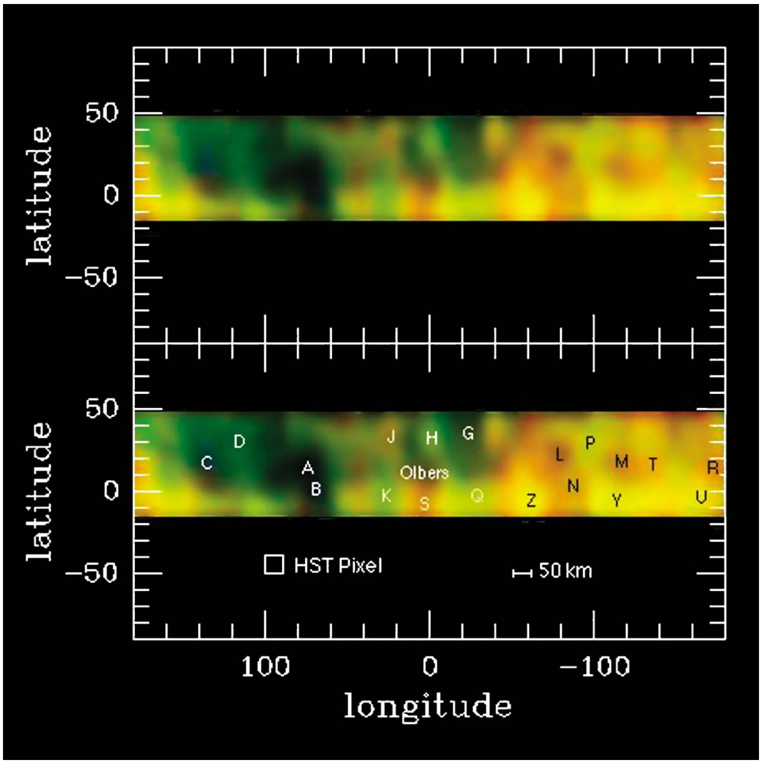

Fig. 5. False-color geologic map of Vesta from HST observations as reported by Binzel et al. (1997). Alphabetic labels correspond to an increasing 1-μm band depth (from Binzel et al., 1997, Figs. 3a and 3b). A subset of these labels (“A,” “B,” “S,” and “Olbers”) is identified in the ground-based images reported herein (Figs. 2 and 3a).

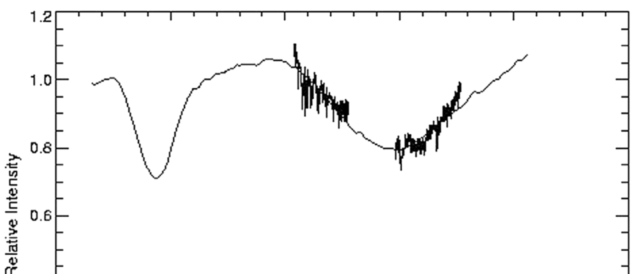

Fig. 6. Disk-averaged Vesta spectra from 153.5° longitude to about 65° longitude in the H and K′ bands from 1.40 to 2.30 μm, corrected for solar flux and normalized to the Gaffey (1997) spectrum (smooth curve). This is a representative spectrum; we found no significant difference between spectra taken at the different locations on Vesta’s disk (Figs. 2 and 3a).

ture near 2 μm. Most importantly, these spectra substantiate and match global composition in a local area.

7. Conclusion

For the first time, spectra and near-infrared images obtained with the Keck AO system of Asteroid 4 Vesta are presented. We have identified albedo features which may be crater-like depressions containing a dark lunar-mare-type basaltic material that is distinct from the general high-albedo eucrite surface material of Vesta. Differences in L′- and K′-band image reflectance data around 45° longitude suggest different physical properties of the same material are present on Vesta’s surface, or that the amount and distribution of pyroxene across the surface is variable, or both. Spectra obtained in this local area show no detectable compositional variation with longitude and match spectra obtained on a global scale.

The unprecedented clarity of the images presented herein will add to the database of 4 Vesta, providing new insights into its albedo variations and mineral compositions. Additionally, these first-ever published AO data for Asteroid 4 Vesta may contribute to a better understanding of the geologic context of the HED meteorites on its surface, as proposed by Drake (2001). The lithologic model presented here matches the reported data and provides a reasonable interpretation of the observed structures. This model can be tested when Dawn arrives at Vesta in 2010 (Russell et al., 2004).

Acknowledgments

The authors thank R. Binzel for useful discussion and for providing data. We also thank Lucy McFadden and an anonymous reviewer for helpful comments on the manuscript. N.E.B.Z. thanks A. Wootton for support during the research and writing of this manuscript. Data presented herein were obtained at the W.M. Keck Observatory, which is operated as a scientific partnership among the California Institute of Technology, the University of California, and the National Aeronautics and Space Administration. The Observatory was made possible by the generous financial support of the W.M. Keck Foundation. This research was supported in part by the STC Program of the National Science Foundation under Agreement No. AST-9876783. The contributions of M. Gaffey to this research were supported by NASA Planetary Geology and Geophysics Program Grants NAG5-13792 and NNG04GJ86G. This research was also supported in part under the auspices of the U.S. Department of Energy at the University of California/Lawrence Livermore National Laboratory under contract No. W-7405-Eng-48, UCRL-JRNL-204154.

References

Binzel, R.P., Gaffey, M.J., Thomas, B.H., Zellner, B.H., Storrs, A.D., Wells, E.N., 1997. Geologic mapping of Vesta from 1994 Hubble Space Telescope images. Icarus 128, 95–103.

Clayton, R.N., Mayeda, T.K., 1996. Oxygen isotope studies of achondrites. Geochim. Cosmochim. Acta 60, 1999–2017.

Colina, L., Bohlin, R.C., Castelli, F., 1996. The 0.12–2.5 micron absolute flux distribution of the Sun for comparison with solar analog stars. Astron. J. 112, 307–315.

Conan, J.-M., Fusco, T., Mugnier, L., Marchis, F., Roddier, C., Roddier, F., 2000. Deconvolution of adaptive optics images: From theory to practice. In: Wizinowich, P. (Ed.), Adaptive Optical Systems Technology. In: Proc. SPIE, vol. 4007. SPIE, Bellingham, WA, pp. 913–924.

Consolmagno, G.J., Drake, M.J., 1977. Composition of the eucrite parent body: Evidence from rare Earth elements. Geochim. Cosmochim. Acta 41, 1271–1282.

Drake, M.J., 1979. Geochemical evolution of the eucrite parent body—Possible nature and evolution of Asteroid 4 Vesta. In: Gehrels, A.M.J. (Ed.), Asteroids. Univ. of Arizona Press, Tucson, AZ, pp. 765–782.

Drake, M.J., 2001. The eucrite/Vesta story. Meteor. Planet. Sci. 36, 501–513.

Gaffey, M.J., 1997. Surface lithologic heterogeneity of Asteroid 4 Vesta. Icarus 127, 130–157.

Gibbard, S.G., de Pater, I., Roe, H.G., Martin, S., Macintosh, B.A., Max, C.E., 2003. The altitude of Neptune cloud features from high-spatial-resolution near-infrared spectra. Icarus 166, 359–374.

Hestroffer, D., Marchis, F., Fusco, T., Berthier, J., 2002. Adaptive optics observations of Asteroid (216) Kleopatra. Astron. Astrophys. 394, 339–343.

Larson, H.P., Fink, U., 1975. Infrared spectral observations of Asteroid 4 Vesta. Icarus 26, 420–427.

Marchis, F., Prangé, R., Fusco, T., 2001. A survey of Io's volcanism by adaptive optics observations in the 3.8-μm thermal band (1996–1999). J. Geophys. Res. 106, 33141–33160.

Marchis, F., de Pater, I., Davies, A.G., Roe, H.G., Fusco, T., Le Mignant, D., Descamps, P., Macintosh, B.A., Prangé, R., 2002. High-resolution Keck adaptive optics imaging of violent volcanic activity on Io. Icarus 160, 124–131.

McCord, T.B., Adams, J.B., Johnson, T.V., 1970. Asteroid Vesta: Spectral reflectivity and compositional implications. Science 168, 1445–1447.

Mittlefehldt, D.W., McCoy, T.J., Goodrich, C.A., Kracher, A., 1998. Non-chondritic meteorites from asteroidal bodies. In: Papike, J.J. (Ed.), Planetary Materials. In: Reviews in Mineralogy, vol. 36. Mineral. Soc. Am., Washington, DC, pp. 4-1–4-195.

Mugnier, L., Fusco, T., Conan, L., 2004. MISTRAL: A myopic edge-preserving image restoration method with application to astronomical adaptive optics corrected long-exposure images. J. Opt. Soc. Am. In press.

Papike, J.J., 1998. Comparative planetary mineralogy: Chemistry of melt-derived pyroxene, feldspar, and olivine. In: Papike, J.J. (Ed.), Planetary Materials. In: Reviews in Mineralogy. Mineral. Soc. Am., Washington, DC.

Prior, G.T., 1916. On the genetic relationship and classification of meteorites. Mineral. Mag. 18, 26–44.

Russell, C.T., 20 colleagues, 2004. Dawn: A journey in space and time. Planet. Space Sci. 52 (5–6), 465–489.

Thomas, P.C., Binzel, R.P., Gaffey, M.J., Storrs, A.D., Wells, N.E., Zellner, B.H., 1997. Impact excavation on Asteroid 4 Vesta: Hubble Space Telescope results. Science 277, 1492–1495.

Wizinowich, P.L., Acton, D.S., Shelton, C., Stomsky, P.J., Gathright, J., Ho, K., Lupton, W., Tsubota, K., Lai, O., Max, C., Brase, J., An, J., Avicola, K., Olivier, S., Gavel, D., Macintosh, B., Ghez, A., Larkin, J., 2000. First light adaptive optics images from the Keck II Telescope: A new era of high angular resolution imagery. Publ. Astron. Soc. Pacific 112 (769), 315–319.

Zellner, B.H., Albrecht, R., Binzel, R.P., Gaffey, M.J., Thomas, P.C., Storrs, D.A., Wells, E.N., 1997. Hubble Space Telescope images of Asteroid 4 Vesta in 1994. Icarus 128, 83–87.